

On role of the atom-cavity detuning in bimodal cavity experiments

D Gon \check{c} a¹ and S Fritzsche^{1,2}

¹ Max-Planck-Institut für Kernphysik, Postfach 103980,
D-69029 Heidelberg, Germany

² Physikalisches Institut der Universität Heidelberg, Philosophenweg 12,
D-69120 Heidelberg, Germany

E-mail: gonta@physi.uni-heidelberg.de

E-mail: s.fritzsche@gsi.de

Abstract. The coherent evolution of the atom-cavity state in bimodal (cavity) experiments has been analyzed for a realistic time-dependence in detuning the atomic transition frequency. Apart from a ‘smooth switch’ of the atomic resonance from one to the second mode of a bimodal cavity, we considered also an additional (effective) interaction between the field modes of the cavity, known as ‘communication channel’. Comparison of our model computations has been made especially with the measurements by Rauschenbeutel *et al* [2001 *Phys. Rev. A* **64** 050301] who demonstrated for the first time the entanglement of the field modes in a bimodal cavity. It is shown that the agreement between the (theoretically) predicted and experimental phase shifts can be improved by allowing a ‘communication’ between the two field modes during a short but finite switch of the atomic transition frequency from one mode to the other. We therefore suggest that the details of the atom-cavity detuning should be taken into account for the future interpretation of bimodal cavity experiments.

PACS numbers: 42.50.Pq, 42.50.Dv, 03.67.Mn

1. Introduction

During the last decades, entanglement has been recognized as a key feature of quantum mechanics that describes not only the correlation in composite quantum systems but is useful also for applications. Since the famous Bohr-Einstein debate and the seminal work of Einstein, Podolsky and Rosen [1] in 1935, indeed, a large number of entanglement studies helped improve our present understanding of nonlocal and nonclassical phenomena as they occur in the microscopic world. In quantum engineering and quantum information theory [2], moreover, entanglement has been found crucial for implementing new (quantum) information protocols, such as superdense coding [3], quantum cryptography [4], or even simple quantum algorithms [5]. However, despite of all progress in the design and description of entangled quantum system, their manipulation and controlled interaction with the environment still remains a great challenge for experiment owing to the fragile nature of most quantum states. Among various other implementations, an excellent control over the light fields and atoms has been achieved especially by using neutral atoms that are coupled to a high-finesse optical cavity [6, 7].

In a recent experiment by Rauschenbeutel and coworkers [8], for example, the two modes of a superconducting (bimodal) cavity were prepared in a maximally entangled state by using circular Rydberg atoms. In this experiment, an entanglement of the two field modes was achieved, by properly adjusting the detuning of the atomic (transition) frequency of the Rydberg atom while it passes through the bimodal cavity. The entangled state produced in the cavity is probed later by a second atom that, after being detected, reveals the coherent evolution of the superposition of the cavity states. The coherence of the (two-qubit) cavity state was demonstrated by varying the delay time after which the probe atom interacts with the cavity. Different delay times give then rise to a oscillation in the final-state probability for the second atom to be found in either the *ground* or *excited* state of the two-level configuration, as supposed for the Rydberg atom. For this final-state probability, an analytical expression was derived by assuming an *idealized* time evolution of the quantum state of both, the photon field and the atoms, throughout the periods of atom-cavity interactions. Despite the high quality of the cavities today, however, such an *ideal* time evolution neglects a number of relevant effects, including the relaxation of the cavity field, the influence of external and internal stray fields, or imperfections due to the cavity mirrors and cavity geometry. In particular the proper matching of the atomic transition frequency to (the frequency of) one or the other cavity mode (the so-called atom-cavity detuning) plays an essential role on the superposition of the cavity states, because the atom has to mediate the interactions between the (cavity) modes while passing through the cavity.

The experiments by Rauschenbeutel *et al* [8] nicely demonstrated how the field modes of a bimodal cavity become entangled or disentangled in a well controlled way by manipulating the (de-) tuning of the atom-cavity interaction. In contrast to the single-mode cavities, the use of bimodal cavities has been found an important step towards the manipulation of complex quantum states and for performing various fundamental tests in quantum theory [9, 10, 11, 12, 13, 14, 15, 16, 17]. For these bimodal cavities, its important to know how (sensitive) the produced cavity state depends on the details and the particular shape of the detuning process. Since the two nearly degenerate frequencies of the cavity modes are fixed by the geometry of the cavity, a detuning of the atom (transition) frequency with regard to one of the field modes automatically affects also the detuning with regard to the other mode. In

our discussions below, we shall often refer to this detuning of the atomic transition frequency (of the Rydberg atoms passing through the cavity) with regard to the field modes briefly as the *atom-cavity detuning*.

In the present work, we examine how the coherent evolution of the cavity state of bimodal cavities, i.e. the superposition of the two cavity modes, is affected by a realistic time-dependence of the atom-cavity detuning and how the atoms, when passing through the cavity, may interact with both cavity modes simultaneously. To exhibit these effects, we make use of two models for the atom-cavity detuning in which the (idealized) *step-wise* detuning of the atomic transition frequency from one to the other cavity mode is replaced by (i) a smooth detuning that happens in a short but finite ('switching') time interval and (ii) a simultaneous interaction of the atom with both cavity modes leading to a wave mixing in the cavity. We shall refer to these models as the (separate) *single-mode interaction* and *communication channel* model. In the latter model, the wave-mixing effects mainly arise due to imperfections of the cavity mirrors that causes the cavity modes to interact (communicate) with each other, cf. Section 2. To follow the time evolution of the atom-cavity interaction, we combine analytical solutions for the Jaynes-Cummings Hamiltonian with numerical simulations, if the atom-cavity interaction is not resonant. For both models, the single-mode interaction and communication channel, the final-state probability for the 'probe' atom to be found in either the ground or excited state is then compared with the experiments in [8]. Using the cavity parameters from these experiments, we show that more realistic assumptions about the shape (and model) of the atom-cavity interaction improves the agreement between the theoretical predictions and experiment. A detailed account of the atom-cavity detuning will therefore play an crucial role also for manipulating and analyzing (more) complex cavity experiments in the future.

In Section 2 we start from the Jaynes-Cummings Hamiltonian to describe the interaction of a two-level atom with the two field modes of a bimodal cavity. For this, we first (re-) derive the expression for the final-state probability in Subsection 2.1 that the probe atom is detected in the excited state by using the matrix formalism and by assuming an idealized *step-wise* change in the atom-cavity interaction. This derivation sets the framework for introducing our more realistic models concerning the shape and explicit form of the atom-cavity interaction in sections 2.2 (single-mode interaction model) and 2.3 (communication-channel). In the latter model, we modify the Jaynes-Cummings Hamiltonian as to allow the atom to interact with both cavity modes simultaneously. In Section 3 then, the predictions from these models for the final-state probability are compared with the data of [8]. In particular, here we display and discuss how the 'switching time' affects the outcome of the experiments. Finally, a few conclusions are given in Section 4.

2. Entanglement of two field modes using a bimodal cavity

The use of the *resonant* atom-cavity interaction regime is the simplest way to generate entangled states between atoms and/or the field modes of a cavity. For a sufficiently high enough quality factor of the cavity mirrors, namely, this regime implies a 'strong' atom-field coupling for which the dissipation of field energy in course of the atom-cavity evolution becomes negligible. Such a small dissipation of the photon field plays a crucial role for engineering of coherent states in the framework of cavity QED. Apart from the quality of the mirrors, the correct matching of the atomic transition frequency

to the frequency of cavity field modes (the so-called *detuning*) is also an important ingredient in order to achieve the resonant atom-cavity interaction regime.

In the following, let us first recall the basic components and notions of the cavity QED experiments by Haroche and coworkers [6]. In these experiments, circular Rydberg atoms in quantum states with principal quantum numbers 50 and 51 are treated as ‘two-level’ systems, being in the ground state $|g\rangle$ or the excited state $|e\rangle$, respectively. Using the Stark shift technique, the frequency of atomic $e \leftrightarrow g$ transition can be tuned in a well controlled way to the nearly degenerate frequencies of the two cavity field modes. If, for the moment, we consider only a single-mode cavity, then the evolution of the atom-cavity state is described (for both, a resonant and non-resonant interaction of the atom with the cavity) by the Jaynes-Cummings Hamiltonian [18]

$$H = \hbar\omega_0 S_z + \hbar\frac{\Omega}{2} (S_+ a_1 + a_1^\dagger S_-) + \hbar\omega_1 \left(a_1^\dagger a_1 + \frac{1}{2} \right), \quad (1)$$

where ω_0 is the atomic $e \leftrightarrow g$ transition frequency, ω_1 the frequency of the cavity field, and Ω the atom-field coupling frequency. In the Hamiltonian (1), moreover, a_1 and a_1^\dagger denote the annihilation and creation operators for a photon in the cavity, acting upon the Fock states $|n\rangle$, while S_- and S_+ are the spin lowering and raising operators that act upon the atomic states $|e\rangle$ and $|g\rangle$, which are the ‘eigenstates’ of the spin operator S_z with eigenvalues $+1/2$ and $-1/2$, respectively. Furthermore, if there is not more than *one* photon in the cavity, the overall atom-field state for a resonant atom-cavity interaction, i.e. for a zero detuning ($0 = \omega_0 - \omega_1$), evolves according to [19]

$$|e, 0\rangle \rightarrow \cos(\Omega t/2)|e, 0\rangle - i \sin(\Omega t/2)|g, 1\rangle, \quad (2a)$$

$$|g, 1\rangle \rightarrow \cos(\Omega t/2)|g, 1\rangle - i \sin(\Omega t/2)|e, 0\rangle. \quad (2b)$$

In the literature, this time evolution of the atom-cavity states is known also as Rabi rotation where t designates the effective atom-cavity interaction time in the laboratory and $(\Omega \cdot t)$ the angle of rotation. Note that neither the state $|e, 1\rangle$ nor $|g, 0\rangle$ appears in the time evolution (2a)-(2b), in line with our physical perception that the ‘photon’ of the $e \leftrightarrow g$ transition is ‘stored’ either by the atom *or* the cavity, but cannot occur twice in the system.

In contrast to single-mode cavities, a bimodal cavity possesses the feature of two nearly degenerate light modes of (usually) orthogonal polarization. Since the frequency of the cavity modes are fixed geometrically by the design of the cavity, its only the atomic frequency that can be tuned by means of external fields in order that the Rydberg atom interacts resonantly with either the first *or* the second cavity field mode. In practise, this detuning is done by applying a well adjusted time-varying electric field across the gap between the cavity mirrors [20] so that the desired (Stark) shift of the atomic transition frequency $\omega_0(t)$ is achieved. By proper adjustment of $\omega_0(t)$, one can induce the desired Rabi rotation of the atomic state interacting either with regard to the first or the second cavity mode [8]. In fact, the development of bimodal cavities has been found important not only for the manipulation of complex quantum states but provides one also with an additional ‘photonic qubit’ in the framework of quantum information that may interact independently with the Rydberg atoms (‘atomic qubits’). Below, we shall denote the two cavity modes by M_1 and M_2 and suppose that they are associated with the frequencies ω_1 and ω_2 , such that $\omega_1 - \omega_2 \equiv \delta > 0$. Since, moreover, the frequencies of the two field modes are fixed, only the atomic $e \leftrightarrow g$ transition frequency can be changed and, as mentioned before,

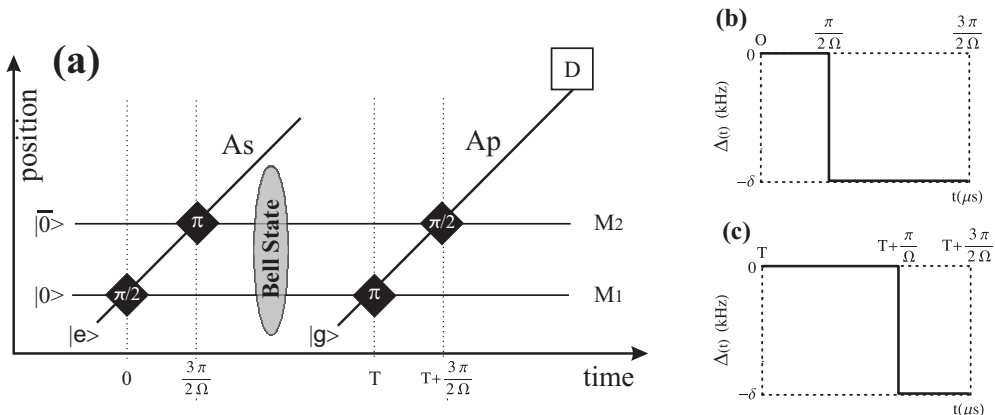


Figure 1. (a) Temporal sequence for producing and observing an entangled state of the two cavity modes. The pictograms are described in the text. The grey ellipse area indicates the place where the entangled state between the cavity modes is obtained. Plots (b) and (c) display the detailed shape of the atom-cavity detuning $\Delta(t) = \omega_0(t) - \omega_1$ during the time periods $[0, \frac{3\pi}{2\Omega}]$ and $[T, T + \frac{3\pi}{2\Omega}]$, respectively.

we shall briefly refer to the (de-)tuning of the atomic frequency with regard to the cavity modes as *atom-cavity detuning*.

For a resonant interaction of the Rydberg atoms with both cavity modes, one need to be able to switch the atomic frequency from one to the other mode. Let $\Delta(t)$ denote the (time-dependent) atom-cavity detuning and let us assume that the atom is in resonance with the cavity mode M_1 for $\Delta(t) \equiv \omega_0(t) - \omega_1 = 0$. It is then in resonance with M_2 for $\Delta(t) = -\delta$. For a sufficiently large frequency shift δ of the two cavity modes, moreover, the atom can be in resonance only with one of the modes and, hence, the time evolution of the (interacting) atom-cavity system $A - M_1 - M_2$ can be ‘divided’ into separate time evolutions owing to the $A - M_1$ or $A - M_2$ resonant interactions [8]. In practise, however, neither mode of the cavity can be *frozen out* completely because of the rather small shift δ ($\approx 2\Omega$ in the experiments in Refs. [6, 8, 9]), the decoherence in the photon field [10] as well as imperfections of the cavity mirrors, i.e. the local roughness and deviations from the spherical geometry. For any theoretical treatment of the decoherence and, especially, the imperfections of the cavity, we must proceed *beyond* the Jaynes-Cummings model (1) by allowing the atom to couple with both cavity modes at the same time [11, 12]. Such a coupling then supports also the coupling between the cavity modes and is therefore referred to as communication channel in the literature [10], cf. Section 2.3. It is the goal of this work to demonstrate how a realistic atom-cavity interaction (coupling) can be analyzed quantitatively and can improve the theoretical predictions on the various probabilities, when compared with experiment [8].

2.1. The step-wise model for detuning the atom-cavity interaction

With this short reminder on the development of bimodal cavities and the Jaynes-Cummings model for the atom-cavity interaction, we are now prepared to discuss all necessary steps for obtaining the coherent superposition of the cavity mode state as

reported recently in the experiments of Rauschenbeutel *et al* [8]. In this reference, an *idealized* time evolution of the atom-cavity system was considered, and it was shown how the two cavity modes can be brought into the maximally entangled Bell state

$$|\Psi\rangle = \frac{1}{\sqrt{2}} (e^{i\psi}|0, \bar{1}\rangle + |1, \bar{0}\rangle) , \quad (3)$$

where $|0\rangle$, $|1\rangle$ denote the Fock states of the cavity mode M_1 , and $|\bar{0}\rangle$, $|\bar{1}\rangle$ the Fock states of mode M_2 , respectively.

In a step-wise model of the atom-cavity interaction, the coherent superposition (3) can be produced as follows. In the derivations below, we shall often apply the matrix representation of the time evolution operators in order to discuss the individual steps. The use of the matrix representation later facilitates also the application of our two models concerning a more realistic atom-cavity interaction. Suppose the cavity is initially ‘empty’, i.e. in the state $|0, \bar{0}\rangle \equiv |0\rangle \times |\bar{0}\rangle$, and is crossed by the (so-called) source atom A_s prepared in the excited state $|e\rangle$. Being within the cavity, this atom is first tuned in resonance with the cavity mode M_1 ($\Delta = 0$) for a Rabi rotation $\Omega t_1 = \pi/2$, and followed by a second rotation $\Omega t_2 = \pi$, now being in resonance with the second mode M_2 ($\Delta = -\delta$). In the step-wise model of the atom-cavity interaction, it is essential that the detuning from mode M_1 to M_2 can be achieved instantaneously, i.e. within a period that is completely negligible to the time of interaction with the individual modes. This idealized sequence of atom-cavity interactions is shown in Figure 1(a) where the Rabi rotations are denoted by the black diamonds, containing the angle of rotation, and where the spatio-temporal evolution can be seen for both, the cavity modes as well as the atoms. Figure 1(b) displays the step-wise change in the atom-cavity detuning from the mode M_1 to M_2 . After the time $\frac{3\pi}{2\Omega}$, the source atom has passed the cavity (and turns out to be de-coupled from the state of the cavity modes).

To understand the time evolution of the atom-cavity system as a whole, we can consider successively the resonant interaction of the atom with the two cavity modes M_1 and M_2 . From Figure 1(b), we see that the (time-dependent) Hamiltonian can be written in the form

$$H_s(t) = \theta_1(t)H_1 + \theta_2(t)H_2 = \begin{cases} H_1(\omega_0 = \omega_1), & 0 \leq t \leq \frac{\pi}{2\Omega} \\ H_2(\omega_0 = \omega_2), & \frac{\pi}{2\Omega} < t \leq \frac{3\pi}{2\Omega} \end{cases} , \quad (4)$$

with the two ‘step functions’

$$\theta_1(t) = 1 - \theta\left(t - \frac{\pi}{2\Omega}\right), \quad \theta_2(t) = \theta\left(t - \frac{\pi}{2\Omega}\right),$$

and where ($\hbar \equiv 1$; $\mu = 1, 2$)

$$H_\mu = \omega_0 S_z + \frac{\Omega}{2} (S_+ a_\mu + a_\mu^\dagger S_-) + \omega_\mu \left(a_\mu^\dagger a_\mu + \frac{1}{2} \right) \quad (5)$$

refers to the Jaynes-Cummings Hamiltonian as discussed above. Following the text by Puri [19], here we introduce the operators

$$N_\mu = a_\mu^\dagger a_\mu + S_z + \frac{1}{2} \quad (6)$$

such that $[H_\mu, N_\mu] = 0$. Especially the last relation enables us in the case that the atom is in resonance with the field mode ($\omega_0 = \omega_\mu$) to cast the Hamiltonian (5) into the equivalent but more convenient form

$$H_\mu = \omega_\mu N_\mu + \frac{\Omega}{2} (a_\mu^\dagger S_- + S_+ a_\mu) . \quad (7)$$

and

$$U_{ij}^{(2)}(t) = \begin{pmatrix} x'(t) & 0 & 0 & 0 & 0 & \bar{y}'(t) & 0 & 0 \\ 0 & \bar{x}'(t) & 0 & 0 & y'(t) & 0 & 0 & 0 \\ 0 & 0 & 1 & 0 & 0 & 0 & 0 & 0 \\ 0 & 0 & 0 & 1 & 0 & 0 & 0 & 0 \\ 0 & \bar{y}'(t) & 0 & 0 & x'(t) & 0 & 0 & 0 \\ y'(t) & 0 & 0 & 0 & 0 & \bar{x}'(t) & 0 & 0 \\ 0 & 0 & 0 & 0 & 0 & 0 & 1 & 0 \\ 0 & 0 & 0 & 0 & 0 & 0 & 0 & 1 \end{pmatrix}, \quad (14)$$

and where

$$x(t) = \bar{x}(t) = \cos\left(\frac{\Omega t}{2}\right), \quad y(t) = \bar{y}(t) = -i \sin\left(\frac{\Omega t}{2}\right). \quad (15)$$

In this notation, the prime refers to the additional phase factor $\square'(t) = e^{i\delta t} \cdot \square(t)$ that arises from the energy difference $\hbar\delta$ of the two cavity modes and is accumulated during the $(A - M_2)$ Rabi rotation [8]. Substituting the expressions (11), (13) and (14) into the wave function (10) and by making use of the initial condition $c_i(0) = \delta_{i1}$, we then obtain at the time $t = \frac{3\pi}{2\Omega}$ two non-zero coefficients

$$c_6\left(\frac{3\pi}{2\Omega}\right) = -\frac{i}{\sqrt{2}}e^{\frac{i\delta\pi}{\Omega}}, \quad c_8\left(\frac{3\pi}{2\Omega}\right) = -\frac{i}{\sqrt{2}}, \quad (16)$$

and, hence, the total wave function (up to an irrelevant phase factor) is

$$|\Psi\left(\frac{3\pi}{2\Omega}\right)\rangle = \frac{1}{\sqrt{2}}\left(e^{\frac{i\delta\pi}{\Omega}}|0, \bar{1}\rangle + |1, \bar{0}\rangle\right)|g\rangle. \quad (17)$$

This wave function is equivalent to those derived in [8] and is the same as displayed above (3). Apparently, the two cavity modes form now are maximally entangled state, while (the state of) the source atom is factorized out.

Unfortunately, the cavity state is inaccessible for direct measurements. In order to ‘prove’ the coherent superposition (17) of the two cavity modes, another (probe) atom A_p has to be sent through the cavity after a time delay $(T - \frac{3\pi}{2\Omega})$. In the experiments in [8], this time delay was chosen between about 0..710 μs . The purpose of the probe atom is to ‘read off’ the state of the cavity modes and to copy this information upon its own state. Similar as the source atom, the probe atom A_p interacts with the cavity during the time interval $[T, T + \frac{3\pi}{2\Omega}]$ being in resonance with the cavity modes M_1 and M_2 as shown in Figure 1(c). Using the arguments from above, the whole time evolution of the atom-cavity system from zero up to the time $(T + \frac{3\pi}{2\Omega})$ is given by applying the evolution matrix

$$U_{ij}\left(T + \frac{3\pi}{2\Omega}\right) = \sum_{k,m,l} U_{ik}^{(5)}\left(\frac{\pi}{2\Omega}\right) U_{km}^{(4)}\left(\frac{\pi}{\Omega}\right) U_{ml}^{(3)}\left(T - \frac{3\pi}{2\Omega}\right) U_{lj}^{(s)}\left(\frac{3\pi}{2\Omega}\right). \quad (18)$$

In this matrix, $U_{ij}^{(s)}$ is given by (11) and refers to the interaction of the cavity with the source atom, while the other matrices $U_{ml}^{(3)}$, $U_{km}^{(4)}$ and $U_{ik}^{(5)}$ describe the three subsequent steps: the *free* time evolution during the time interval $[\frac{3\pi}{2\Omega}, T]$

$$U_{ij}^{(3)}(t) = \text{diag}\{1, 1, 1, 1, 1, e^{i\delta t}, 1, 1\}, \quad (19)$$

which is diagonal in the basis (8a)-(8b) and where a relative phase shift $e^{i\delta t}$ is accumulated due to the energy difference $\hbar\delta$ of the two cavity modes. Afterwards,

during the interval $[T, T + \frac{3\pi}{2\Omega}]$, the further evolution of the atom-cavity system is driven by the Hamiltonian [cf. Figure 1(c)]

$$H_p(t) = \theta_3(t)H_1 + \theta_4(t)H_2 = \begin{cases} H_1, & T \leq t \leq T + \frac{\pi}{\Omega} \\ H_2, & T + \frac{\pi}{\Omega} < t \leq T + \frac{3\pi}{2\Omega} \end{cases}. \quad (20)$$

Since the atom-cavity interaction is as well described by the Jaynes-Cummings Hamiltonian (7), the matrices $U_{ij}^{(4)}(t)$ and $U_{ij}^{(5)}(t)$ coincides with the matrices (13) and (14), except that in $U_{ij}^{(4)}(t)$ the relative phase $e^{i\delta t}$ occurs. Including this phase factor, $U_{ij}^{(4)}(t)$ then becomes

$$U_{ij}^{(4)}(t) = \begin{pmatrix} x(t) & 0 & 0 & 0 & 0 & 0 & 0 & y(t) \\ 0 & \bar{x}(t) & 0 & 0 & 0 & 0 & \bar{y}(t) & 0 \\ 0 & 0 & 1 & 0 & 0 & 0 & 0 & 0 \\ 0 & 0 & 0 & 1 & 0 & 0 & 0 & 0 \\ 0 & 0 & 0 & 0 & 1 & 0 & 0 & 0 \\ 0 & 0 & 0 & 0 & 0 & e^{i\delta t} & 0 & 0 \\ 0 & y(t) & 0 & 0 & 0 & 0 & x(t) & 0 \\ \bar{y}(t) & 0 & 0 & 0 & 0 & 0 & 0 & \bar{x}(t) \end{pmatrix}. \quad (21)$$

Having the complete time evolution (18), we can easily determine the probability $P(T)$ to find the probe atom in the excited state $|e\rangle$, after it has crossed the cavity and hit the detector D. This is the (final-state) probability that has been measured during the experiment [8] and that provides us with the information about the superposition of the cavity mode states (17). In practise, of course, the atom-cavity interaction is not *ideal* and has to be replaced by some realistic model for the atom-cavity interaction. For the idealized sequence of interaction, however, the (complete) time evolution owing to the matrix (18) at the time $t = \frac{3\pi}{2} + T$ implies only the two non-zero coefficients

$$c_1 \left(\frac{3\pi}{2} + T \right) = -\frac{1}{2} e^{\frac{i\delta\pi}{2\Omega}} \left(1 + e^{\frac{i\delta\pi}{2\Omega}} e^{i\delta T} \right),$$

$$c_6 \left(\frac{3\pi}{2} + T \right) = \frac{i}{2} e^{\frac{i\delta\pi}{2\Omega}} \left(1 - e^{\frac{i\delta\pi}{2\Omega}} e^{i\delta T} \right);$$

and, hence, the final-state probability to find A_p in the excited state is simply

$$P(T) = \left| c_1 \left(\frac{3\pi}{2} + T \right) \right|^2 = \frac{1 + \cos(\omega T + \phi)}{2}. \quad (22)$$

Obviously, this probability oscillates between zero and one with the frequency $\omega \equiv \delta$ and with the phase (shift) $\phi \equiv \pi\delta/2\Omega$. In the experiments by Rauschenbeutel *et al* [8] and Raimond *et al* [6], the shift between the cavity mode frequencies takes the value $\delta/2\pi = 128.3$ kHz, while the atom-cavity coupling constant is $\Omega/2\pi = 47$ kHz.

2.2. Changing the atom-cavity detuning in a smooth way

In the previous Subsection, it was shown how the (two) cavity modes become entangled with each other by detuning the atom-cavity interaction in a proper way. For a step-wise detuning $\Delta(t)$ as displayed in figures 1(b) and (c), this leads to the maximally entangled state (17) of the two cavity modes after the source atom has passed through the cavity, leaving the atom factorized out in a product state. This ‘sudden’ change in the detuning $\Delta(t)$ is however not physically feasible, and further analysis is required

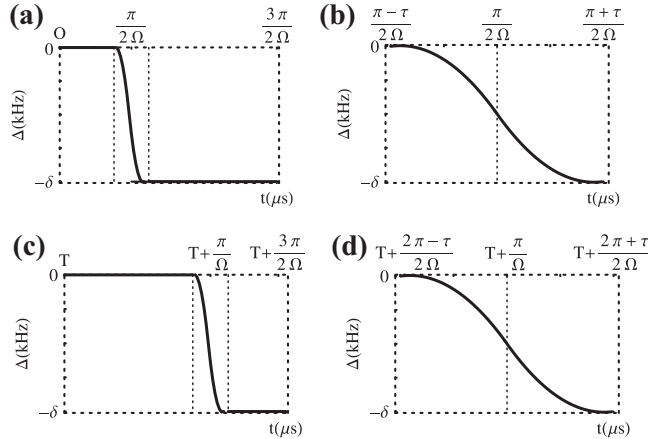


Figure 2. Temporal sequence of the atom-cavity detuning if the interaction of the atom is changed smoothly from one to the other cavity mode. Plot (a) display the atom-cavity detuning $\Delta(t) = \omega_0(t) - \omega_1$ during the interval $[0, \frac{3\pi}{2\Omega}]$ where the transition frequency of the source atom is detuned from the cavity mode M_1 to the mode M_2 ; this ‘smooth change’ is inflated in plot (b) for the interval $[\frac{\pi-\tau}{2\Omega}, \frac{\pi+\tau}{2\Omega}]$. The plots (c) and (d) display the same but for the atom-cavity detuning $\Delta(t) = \omega_0(t) - \omega_1$ during the time interval $[T, T + \frac{3\pi}{2\Omega}]$, i.e. when the cavity interacts with the probe atom.

to understand how the evolution of cavity states is affected by a more realistic time-dependence of the detuning. In this sections, therefore, we shall consider a smooth ‘switch’ from the $A_{s/p} - M_1$ to the $A_{s/p} - M_2$ resonant interaction within a *finite* time period, which we will denote by τ . For instance, according to the experimental setup [8] this period is of the length $\tau/\Omega \leq 1 \mu s$, which corresponds to $\sim 7\%$ of the overall $\frac{3\pi}{2\Omega}$ interaction time of the atom with the cavity, or about an angle $\frac{\pi}{10}$ in units of Rabi rotations, which is not anymore negligible (as we considered in the previous model). Below, we shall assume a smooth behavior for this finite switch as displayed in figures 2(a) and (c), where the cavity is non-resonant to the source atom during the interval $[\frac{\pi-\tau}{2\Omega}, \frac{\pi+\tau}{2\Omega}]$ and with the probe atom during $[T + \frac{2\pi-\tau}{2\Omega}, T + \frac{2\pi+\tau}{2\Omega}]$, respectively. This smooth switch of the atomic resonance from one to the other cavity mode can be described mathematically by the Hamiltonian

$$H_s^\tau(t) = \begin{cases} H_1, & 0 \leq t \leq \frac{\pi-\tau}{2\Omega} \\ H_-(t), & \frac{\pi-\tau}{2\Omega} < t \leq \frac{\pi}{2\Omega} \\ H_+(t), & \frac{\pi}{2\Omega} < t \leq \frac{\pi+\tau}{2\Omega} \\ H_2, & \frac{\pi+\tau}{2\Omega} < t \leq \frac{3\pi}{2\Omega} \end{cases}, \quad (23)$$

where H_1 and H_2 are the resonant Jaynes-Cummings Hamiltonian (7) from above, and where $H_-(t)$ and $H_+(t)$ are given by

$$H_-(t) = S_z \Delta(t) + \omega_1 N_1 + \frac{\Omega}{2} (a_1^+ S_- + S_+ a_1), \quad (24)$$

$$H_+(t) = S_z [\Delta(t) + \delta] + \omega_2 N_2 + \frac{\Omega}{2} (a_2^+ S_- + S_+ a_2). \quad (25)$$

Here, the superscript ‘ τ ’ in (23) is introduced in order to distinguish the Hamiltonian (23) from that of the step-wise detuning (4). Note that, for the present smooth change of the atom-cavity detuning, H_1 and $H_-(t)$ together describe the (time) evolution of the $A_s - M_1$ interaction up to the time $\frac{\pi}{2\Omega}$. That is the resonant part of the atom-cavity interaction due to H_1 is shortened by the time interval $\frac{\tau}{2\Omega}$, while the remaining time up to $\frac{\pi}{2\Omega}$ follows the *non-resonant* Jaynes-Cummings Hamiltonian $H_-(t)$ in line with figure 2(a)-(b). Similarly, the $A_s - M_2$ interaction is first non-resonant and modeled by the Hamiltonian $H_+(t)$ for the interval $[\frac{\pi}{2\Omega}, \frac{\pi+\tau}{2\Omega}]$, and becomes later resonant with the cavity mode M_2 , as seen on figure 2(c)-(d). Obviously, the Hamiltonian (23) can be understood also as an extension of the ‘step-wise’ model from Section 2.1 by introducing an additional short period for the non-resonant atom-cavity interaction. For the Hamiltonian (23), therefore, the time evolution matrix still factorizes and can be expressed at $t = \frac{3\pi}{2\Omega}$ as

$$U_{ij}^{(s)}\left(\frac{3\pi}{2\Omega}\right) = \sum_{k,l,m} U_{ik}^{(2)}\left(\frac{\pi}{\Omega} - \frac{\tau}{2\Omega}\right) U_{kl}^{(+)}\left(\frac{\tau}{2\Omega}\right) U_{lm}^{(-)}\left(\frac{\tau}{2\Omega}\right) U_{mj}^{(1)}\left(\frac{\pi - \tau}{2\Omega}\right) \quad (26)$$

where the matrices $U_{ij}^{(1)}(t)$ and $U_{ij}^{(2)}(t)$ are the same as in (13) and (14), and where the matrix $U_{ij}^{(-)}(t)$ has still the form (13) but with $x(t)$, $\bar{x}(t)$, $y(t)$, and $\bar{y}(t)$ now being solutions of the differential equations [19]:

$$i \frac{dy(t)}{dt} = \frac{\Omega}{2} \bar{x}(t) + \frac{1}{2} \Delta(t) y(t), \quad i \frac{d\bar{x}(t)}{dt} = \frac{\Omega}{2} y(t) - \frac{1}{2} \Delta(t) \bar{x}(t), \quad (27)$$

$$i \frac{dx(t)}{dt} = \frac{\Omega}{2} \bar{y}(t) + \frac{1}{2} \Delta(t) x(t), \quad i \frac{d\bar{y}(t)}{dt} = \frac{\Omega}{2} x(t) - \frac{1}{2} \Delta(t) \bar{y}(t). \quad (28)$$

Analogue, the matrix $U_{ij}^{(+)}(t)$ has the form (14) but with functions $x(t)$, $\bar{x}(t)$, $y(t)$, and $\bar{y}(t)$ that are obtained from (27) and (28) by replacing $\Delta(t) \rightarrow \Delta(t) + \delta$.

No exact analytic solutions are known for the relations (27)–(28). Therefore, in order to derive the time evolution matrix (26), we need to solve these equations for $x(t)$, $\bar{x}(t)$, $y(t)$, and $\bar{y}(t)$ numerically up to $t = \frac{\tau}{2\Omega}$, and then to substitute their values into the matrices $U_{ij}^{(\pm)}(t)$. As discussed above, the final-state probability to find the probe atom in the state $|e\rangle$ is obtained by performing a similar procedure for the $A_p - M_1 - M_2$ interaction during the time interval $[T, T + \frac{3\pi}{2\Omega}]$. During the time $[\frac{3\pi}{2\Omega}, T]$, of course, the ‘free’ evolution of the cavity state still follows the trivial matrix (19). Putting all these pieces together, hence, the complete time evolution of the wave function for such a smooth change in the atom-cavity interaction is described by the matrix

$$U_{ij}^{(\tau)}\left(T + \frac{3\pi}{2\Omega}\right) = \sum_{k,m,l,n,p} U_{ik}^{(5)}\left(\frac{\pi - \tau}{2\Omega}\right) U_{km}^{(+)}\left(\frac{\tau}{2\Omega}\right) U_{ml}^{(-)}\left(\frac{\tau}{2\Omega}\right) U_{ln}^{(4)}\left(\frac{\pi}{\Omega} - \frac{\tau}{2\Omega}\right) \\ \times U_{np}^{(3)}\left(T - \frac{3\pi}{2\Omega}\right) U_{pj}^{(s)}\left(\frac{3\pi}{2\Omega}\right), \quad (29)$$

and where the matrices $U_{ij}^{(3)}(t)$, $U_{ij}^{(4)}(t)$, $U_{ij}^{(5)}(t)$, and $U_{ij}^{(s)}(t)$ coincide with matrices (19), (21), (14), and (26), respectively. For the initial condition $c_i(0) = \delta_{i1}$, the final-state probability in model is again

$$P_\tau(T) = |\langle \mathbf{V}_1 | \Psi_\tau(T) \rangle|^2 = \left| c_1 \left(T + \frac{3\pi}{2\Omega} \right) \right|^2 \quad (30)$$

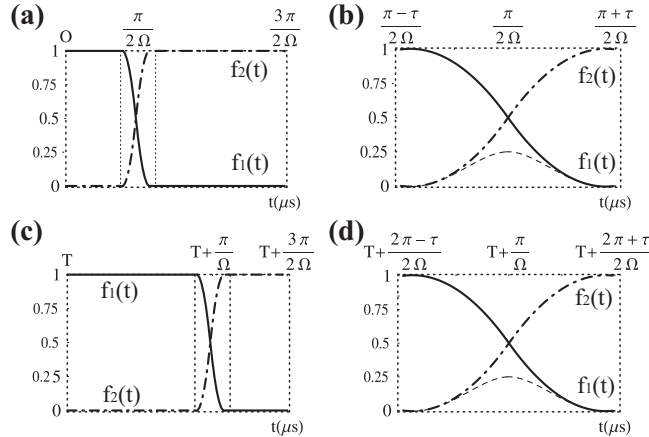


Figure 3. Temporal shape of the dimensionless functions $f_1(t)$ and $f_2(t)$ that describe the contribution of the $A_{s/p} - M_1$ interaction (solid line) and the $A_{s/p} - M_2$ interaction (dot-dashed line) to the total Hamiltonian of the atom-cavity interaction. Plots (b) and (d) display also temporal shape of the product $f_1(t) \cdot f_2(t)$ (dashed line) that describes the contribution of ‘communication channel’ to the total Hamiltonian of the atom-cavity interaction.

which, however, cannot be given in a closed form because of the need for solving the functions $x(t)$, $\bar{x}(t)$, $y(t)$, and $\bar{y}(t)$ numerically in the various matrices. Like the cosine function (22) from the step-wise model, this probability still oscillates between zero and one with the frequency ω_τ and phase ϕ_τ . In the Section 3, we display and discuss how the frequency and phase (shift) behave as function of the ‘switching’ parameter τ , i.e. the time for which the cavity is non-resonant to the atom.

2.3. Communication channel model: Allowing the mutual interaction of the cavity modes

Up to the present, we have always assumed that, at a given time t , the atom interacts either with the cavity mode M_1 or the mode M_2 , implying a sudden change in the interaction from one cavity mode to the other. In our notation above, this means that the overall atom-cavity interaction is understood as a set of *pure* $A_{s/p} - M_1$ or $A_{s/p} - M_2$ (non)resonant interactions. However notice that at the time $t = \frac{\pi}{2\Omega}$ in figure 2(b), for instance, the atomic transition frequency is equally far from the (nearly degenerate) frequencies of both cavity modes and, hence, we expect the atom to ‘feel’ the (non-resonant) contribution of M_1 and M_2 simultaneously. As additional sources for such a simultaneous interaction also serve the imperfections of the mirrors, stray fields, decoherence, etc. Finally, this simultaneous interaction also implies a mutual interaction among the cavity modes to which one therefore refers as a communication channel [10, 19].

To describe this ‘communication’ between the two cavity modes, we need to proceed *beyond* the Jaynes-Cummings model in order to allow the atom to couple with both cavity modes at the same time. In addition, in order to preserve the ‘correspondence’ with the previous two models, this simultaneous interaction must happen only inside the time intervals $[\frac{\pi-\tau}{2\Omega}, \frac{\pi+\tau}{2\Omega}]$ and $[T + \frac{2\pi-\tau}{2\Omega}, T + \frac{2\pi+\tau}{2\Omega}]$, given

by the same ‘switching’ parameter τ as in Section 2.2. Below, we shall model the total (source) atom-cavity interaction within the interval $[0, \frac{3\pi}{2\Omega}]$ by means of the time-dependent Hamiltonian

$$\tilde{H}_s^\tau(t) = \begin{cases} H_1, & 0 \leq t \leq \frac{\pi-\tau}{2\Omega} \\ H_\times(t), & \frac{\pi-\tau}{2\Omega} < t \leq \frac{\pi+\tau}{2\Omega} \\ H_2, & \frac{\pi+\tau}{2\Omega} < t \leq \frac{3\pi}{2\Omega} \end{cases} \quad (31)$$

with

$$H_\times(t) = f_1(t)H_-(t) + f_2(t)H_+(t) + f_1(t)f_2(t)H_I, \quad (32)$$

$$H_I = \lambda (a_1^\dagger a_2 + a_2^\dagger a_1), \quad (33)$$

and where H_μ and $H_\pm(t)$ denote the Hamiltonians (7) and (24)-(25), respectively. The temporal behavior of the detuning $\Delta(t)$ used in $H_\pm(t)$ is the same as we considered in the previous section and which is displayed in Figure 2. The two (dimensionless) functions $f_1(t)$ and $f_2(t)$ displayed in Figure 3(a), thus determine the contribution of the non-resonant Jaynes-Cummings Hamiltonians $H_\pm(t)$ and the communication channel Hamiltonian H_I to the overall time-dependent Hamiltonian (31). In this model, again, the resonant $A_s - M_1$ and $A_s - M_2$ interactions are shortened by time interval τ/Ω and the evolution of the (atom-cavity) state is governed by the Hamiltonian $H_\times(t)$ with the non-resonant part $H_\pm(t)$ and the communication channel H_I . The Hamiltonian H_I is the simplest expression that fulfills the above requirements and preserves the cavity field energy. The contribution of H_I to the Hamiltonian $H_\times(t)$ is given by the time-dependent dimensionless product $f_1(t)f_2(t)$. The shape of this coupling term is displayed in Figure 3(b) by a dashed line, which has its maximal value $1/4$ at $t_{max} = \pi/2\Omega$. Making use of the functions $f_\mu(t)$ in the Hamiltonian (31), we expect to describe the atom-cavity interaction during the switching period τ/Ω in a realistic fashion. Moreover, below we shall consider also the coupling strength λ of the cavity modes such that the ‘effective’ coupling $\lambda f_1(t)f_2(t)$ satisfies the relation

$$\lambda f_1(t_{max})f_2(t_{max}) = \Omega. \quad (34)$$

The meaning of the last relations can be understood as follows: The strongest $M_1 - M_2$ effective coupling should be (or, at least, should not exceed) the composition of the $A_s - M_1$ and $A_s - M_2$ couplings given by the values of $\Omega/2$, respectively. A simple calculation implies the value of λ to be of the order of ~ 1 MHz. For this value, indeed, a good agreement with the experimental data of [8] has been found within the expected time ($\tau/\Omega \leq 1 \mu s$), i.e. for that time which is needed to ‘switch’ the atomic frequency between the two cavity modes (see Section 3). Therefore, the Hamiltonian (31) exposes the right ‘correspondence’ property with regard to the models we have introduced in the previous two Sections. This can be readily seen if we assume $f_1(t) = \theta_1(t)$ and $f_2(t) = \theta_2(t)$; then, expression (31) reduces to the Hamiltonian $H_s^\tau(t)$ (23) and, if we additionally impose the limit $\tau \rightarrow 0$, the Hamiltonian (31) simplifies to $H_s(t)$ in expression (4).

The time evolution matrix at $t = \frac{3\pi}{2\Omega}$ as described by the Hamiltonian (31) is given by

$$\tilde{U}_{ij}^{(s)}\left(\frac{3\pi}{2\Omega}\right) = \sum_{k,l} U_{ik}^{(2)}\left(\frac{\pi}{\Omega} - \frac{\tau}{2\Omega}\right) U_{kl}^{(\times)}\left(\frac{\tau}{\Omega}\right) U_{lj}^{(1)}\left(\frac{\pi-\tau}{2\Omega}\right), \quad (35)$$

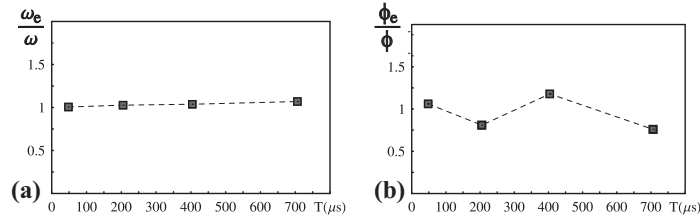


Figure 4. The relative frequency (a) and phase (b) of the final-state probability as obtained experimentally and displayed for the four time intervals I_ν in [8]. The values from the experiment are displayed by dots and are combined by a dashed line in order to guide the eyes of the reader. See text for further explanations.

where $U_{ij}^{(1)}(t)$ and $U_{ij}^{(2)}(t)$ refer to the expressions (13) and (14), and where the matrix elements of $U_{ij}^{(\times)}(t)$ must fulfill the Schrödinger equation

$$i \frac{dU_{ij}^{(\times)}(t)}{dt} = \sum_k \langle \mathbf{V}_i | H_\times(t) | \mathbf{V}_k \rangle U_{kj}^{(\times)}(t). \quad (36)$$

This set of differential equations cannot be solved analytically and need to be integrated numerically during the interval $t = \frac{\tau}{\Omega}$. Indeed, a similar procedure has to be performed later also for the $A_p - M_1 - M_2$ interaction during the time $[T, T + \frac{3\pi}{2\Omega}]$ as seen from figures 3(c),(d) and figures 2(c),(d). Combining the pieces together, the complete time evolution of the atom-cavity interaction therefore becomes

$$\begin{aligned} \tilde{U}_{ij}^{(\tau)} \left(T + \frac{3\pi}{2\Omega} \right) &= \sum_{k,m,l,n} U_{ik}^{(5)} \left(\frac{\pi - \tau}{2\Omega} \right) U_{km}^{(\times)} \left(\frac{\tau}{\Omega} \right) U_{ml}^{(4)} \left(\frac{\pi}{\Omega} - \frac{\tau}{2\Omega} \right) \\ &\quad \times U_{ln}^{(3)} \left(T - \frac{3\pi}{2\Omega} \right) \tilde{U}_{nj}^{(s)} \left(\frac{3\pi}{2\Omega} \right), \end{aligned} \quad (37)$$

where the matrices $U_{ij}^{(3)}(t)$, $U_{ij}^{(4)}(t)$, $U_{ij}^{(5)}(t)$, and $\tilde{U}_{ij}^{(s)}(t)$ coincide with the matrices (19), (21), (14), and (35) respectively. Moreover, the final-state probability is given for the initial conditions $c_i(0) = \delta_{i1}$ by

$$\tilde{P}_\tau(T) = |\langle \mathbf{V}_1 | \tilde{\Psi}_\tau(T) \rangle|^2 = \left| c_1 \left(T + \frac{3\pi}{2\Omega} \right) \right|^2. \quad (38)$$

Although no closed expression can be given for this probability (due to the numerical parts in the time evolution), it still oscillates between zero and one with the frequency $\tilde{\omega}_\tau$ and the phase $\tilde{\phi}_\tau$ that is different from the two other models in Sections 2.1 and 2.2. In the next Section, we shall discuss how these frequency and phase (shifts) behave as functions of the ‘switching’ parameter τ .

3. Comparison with experiment and discussion

The expression (22) of the final-state probability describes the time evolution of an idealized experiment [8] with a step-wise change in the resonant interaction between the two cavity modes. This expression neglects of course a number of additional effects, such as the cavity field relaxation, the influence of external stray fields, or imperfections due to the cavity mirrors and cavity geometry. The most significant

distortion of the idealized probability in (22) is given by the cavity field relaxation during the interval $[\frac{3\pi}{2\Omega}, T]$, i.e. during the ‘free’ evolution of the cavity field, since during the $A_s - M_1 - M_2$ and $A_p - M_1 - M_2$ interactions, the system evolves in the strong coupling (resonant) regime, and hence, the dissipation of the cavity energy is negligible. This field relaxation mainly arises from the interaction of the cavity with the environment and its effect on the final-state probability (22) has been investigated recently by de Magalhaes and Nemes [10]. In this reference, the environmental degrees of freedom were modeled by a infinite set of harmonic oscillators whose annihilation (creation) operators c_b (c_b^+) are coupled linearly to the Hamiltonian of the cavity field modes as follows

$$H(t) = \begin{cases} H_s(t), & 0 \leq t \leq \frac{3\pi}{2\Omega} \\ H_{coupled}, & \frac{3\pi}{2\Omega} < t < T \\ H_p(t), & T \leq t \leq T + \frac{3\pi}{2\Omega} \end{cases} \quad (39)$$

with

$$H_{coupled} = \sum_{\mu=1,2} \omega_{\mu} a_{\mu}^{\dagger} a_{\mu} + \sum_b^{\infty} (\omega_b c_b^{\dagger} c_b + \gamma_{1b} [a_1 c_b^{\dagger} + a_1^{\dagger} c_b] + \gamma_{2b} [a_2 c_b^{\dagger} + a_2^{\dagger} c_b]),$$

and where ω_b describe the frequencies and $\gamma_{\mu b}$ the respective coupling constants. Following [10], the final-state probability can be cast into the form

$$P(T) = A(T) \frac{1 + \cos(\omega T + \phi)}{2} + B(T), \quad (40)$$

with

$$A(T) = e^{-(\alpha+\beta)\xi}, \quad B(T) = \frac{e^{-2\alpha\xi} + e^{-2\beta\xi} - 2e^{-(\alpha+\beta)\xi}}{4}, \quad \xi \equiv T - \frac{3\pi}{2\Omega}, \quad (41)$$

and in which α, β denote the dissipation constants of the cavity, while the frequency ω and phase ϕ coincides with those of expression (22). In fact, the probability (40) has been found in a good agreement with the experimental data of [8] with regard to the amplitude and frequency of the oscillations. However, less agreement was obtained for the phase shift of the final-state probability as given by $\phi \equiv \pi\delta/2\Omega$. Note that, according to (40), the two arguments of the *cosine*: ω and ϕ , are independent of the dissipation constants α and β of the cavity. Therefore, we can describe the frequency and phase shifts in the final-state probability separately from the damping of the signal, as given by functions (41). For the two models (30) and (38), indeed, we will show below that a finite ‘switch’ (Section 2.2) and the communication between the cavity modes (Section 2.3) mainly affects the phase of the amplitude (40), as have been prognosticated in [10]. Therefore, combined with the ‘damping functions’ (41), our investigations enables us to further improve the agreement with experiment.

We now compare the predictions for the frequency and phase of the final-state probability, obtained with the models from Section 2, with those from experiment [8]. In these measurements, the probability for detecting the probe atom A_p in the excited state $|e\rangle$ was recorded and displayed for the four time intervals $I_1 = [48; 57] \mu s$, $I_2 = [200; 207] \mu s$, $I_3 = [400, 408] \mu s$, and $I_4 = [699, 706] \mu s$, respectively. From the observed probability (cf. Figures 2(a)-(d) in [8]), the four ‘experimental’ frequencies and phases have been extracted by a fit to the analytical function (40), where the cosine arguments have been considered as unknown values, separately for each time interval I_{ν} ($\nu = 1, \dots, 4$), and are displayed by the dots in figure 4. For the sake of convenience, moreover, these experimental data were normalized to the reference

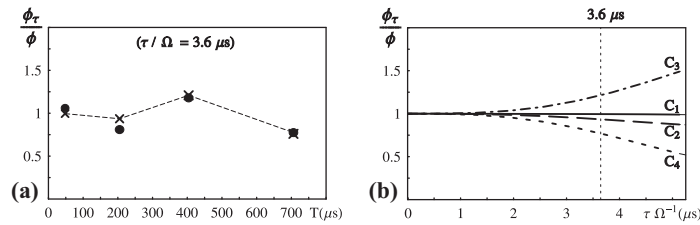


Figure 5. Comparison of the relative phase $\frac{\phi_\tau}{\phi}$ for a smooth change of the atom-cavity detuning (cf. Section 2.2) with experiment. (a) Results are shown for the ‘switching’ parameter $\tau\Omega^{-1} = 3.6 \mu s$, for which the best agreement with the experimental data (dots) is found. The theoretical values (crosses) are joined by dashed lines to guide the eyes of the reader. Figure (b) displays the relative phase $\frac{\phi_\tau}{\phi}$ as a function of τ (curves C_ν). Every curve corresponds to a phase ϕ_τ as obtained for the time intervals I_ν . The vertical dashed line indicates the τ value from plot (a).

frequency $\omega \equiv \delta = 2\pi \times 128.3$ kHz and phase $\phi \equiv \pi\delta/2\Omega = 4.29$ of the ‘idealized’ probability (22). As seen from figure 4, clear deviations of the extracted experimental phase ϕ_e occur with regard to the reference phase ϕ .

To understand how a smooth change in the atom-cavity detuning $\Delta(t)$ affects the frequency and phase of the predicted final-state probability, a number of steps have to be carried out for both models of Sections 2.2 and 2.3: (i) to evaluate numerically the final-state probability $P_\tau(T)$ or $\tilde{P}_\tau(T)$ for the time delay intervals I_ν from the experiment; (ii) to fit the numerical results from step (i) to the analytical function (40) in order to extract the cosine arguments for every time interval; and (iii) to repeat the previous two steps for different values of the ‘switching’ parameter τ . The (cosine) arguments obtained from this procedure can then be compared to the experimental dots from figure 4 in order to determine the parameter τ that agrees better with the experiment.

Figure 5 compares the relative phase ϕ_τ/ϕ for a smooth change of the atom-cavity detuning as modeled in Section 2.2. In Figure 5(a), results are shown for the ‘switching’ parameter $\tau/\Omega = 3.6 \mu s$, for which the best agreement with the experimental data (dots) is found. In addition, figure 5(b) displays the relative phase $\frac{\phi_\tau}{\phi}$ as a function of τ for each time intervals I_ν . As seen from this Figure, our mixed analytic-numerical treatment of the atom-cavity state gives (as expected) the same final-state probability (22) in the limit $\tau \rightarrow 0$. Note that the differences between ω_τ and ω is about two orders of magnitude smaller than the differences in the phases (and are therefore not displayed here). This confirms that the frequency of the final-state probability is less sensitive to ‘undesired’ effects in the atom-cavity interaction than the phase shift. The best agreement between our predictions and experiment is found for a ‘switching time’ $\tau/\Omega = \bar{\tau}/\Omega = 3.6 \mu s$ that is far outside of what is expected for the switch of the atomic transition frequency from one to the other cavity mode in the experiment [8]. Therefore, despite of its rather large effect on the phase-shift of the final-state probability, the finite switching time cannot explain the observations from the experiment as taken alone.

In the communication channel model from Section 2.3, in contrast, the atom interacts for a short period with both cavity modes simultaneously, leading to an effective ‘communication’ between the cavity modes. Figure 6(a) displays again the

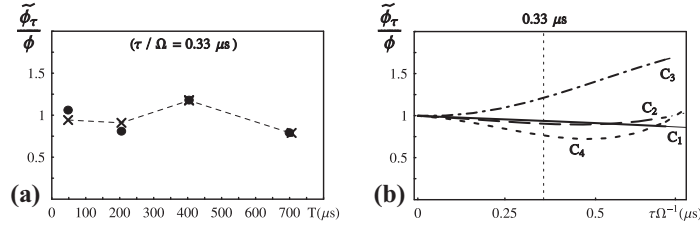


Figure 6. The same as figure 5 but for the communication-channel model in Section 2.3, $\frac{\tilde{\phi}_\tau}{\phi}$. (a) Results are shown again for the ‘switching’ parameter $\tau \Omega^{-1} = 0.33 \mu s$ with the best agreement with the experimental data (dots). The theoretical values (crosses) are joined by dashed lines to guide the eyes of the reader. Figure (b) displays the relative phase $\frac{\tilde{\phi}_\tau}{\phi}$ as a function of τ (curves C_ν). Every curve corresponds to a phase $\tilde{\phi}_\tau$ as obtained for the time intervals I_ν . The vertical dashed line indicates the τ value from plot (a).

relative phase $\tilde{\phi}_\tau / \phi$ for that switching parameter, $\tau / \Omega = 0.33 \mu s$, for which the best agreement with the experimental data (dots) is found. This value nicely fits to the expected time that is needed to ‘switch’ the atomic frequency between the two cavity modes. Moreover, the relative phase $\tilde{\phi}_\tau / \phi$ as function of τ is shown in figure 6(b) for each time intervals I_ν separately. We therefore conclude that a finite switch together with an effective communication of the two cavity modes, i.e. the model of the communication channel, is appropriate for describing the atom-cavity interaction when the atom passes through the cavity.

Let us mention once more that numerical simulations were performed only ‘while’ the atomic frequency is switched between the cavity modes ($\tau \Omega^{-1} \leq 1 \mu s$), both for the single-mode (Section 2.2) as well as the communication-channel model (Section 2.3). For all other periods, the time evolution of the atom-cavity state was followed analytically (15) owing to a purely resonant atom-cavity interaction. The slight deviation between the predicted and observed phases [Figures 6(a) and 5(a)] clearly indicate that there is no perfect agreement with the experimental data. However, no error bars has been given on the final-state probability in [8], and hence this slight disagreement should be later on refined in accordance with error bars which occur in cavity QED experiments.

4. Summary and outlook

The coherent evolution of the atom-cavity state in bimodal (cavity) experiments has been analyzed for a realistic time-dependence of the detuning of the atomic transition frequency. Apart from a ‘smooth switch’ of the atomic resonance from one to the other cavity mode during a short but finite time interval (Section 2.2), we considered also an additional (effective) interaction, a so-called communication channel, between the two cavity modes (Section 2.3). While, in the former case, the atom interacts at any time with just one mode of the photon field, either resonantly or non-resonantly, a simultaneous interaction with both field modes is modeled by means of the communication channel. The outcome of the experiment is the final-state probability for that the probe atom is observed in the (excited) Rydberg state; this probability is analyzed by combining the analytical solution of the Jaynes-Cummings

Hamiltonian with numerical simulations for all those time intervals during which the atom-cavity interaction is tuned from one cavity mode to the other.

Comparison of our model computations have been made especially with the recent measurements by Rauschenbeutel and coworkers [8]. To this end, a series of computations have been carried out for the final-state probability as function of the delay time T and for different (realistic) choices of the ‘switching time’ τ , the model parameter, during which the atom is non-resonant to the cavity modes. Making use of typical cavity parameters as reported in [8], it is demonstrated that the agreement between the predicted and experimental phase can be improved by allowing a ‘communication’ between the two cavity modes, cf. Figures 5 and 6. Together with the recent study by de Magalhaes and Nemes [10], who investigated the damping of the probability amplitude due to the coupling of the cavity to the environment, the use of the communication channel from above brings the theoretical predictions in good agreement with experiment. For the interpretation of future bimodal experiments, therefore, it seems appropriate to take into account both, the decoherence as well as the details of the atom-cavity detuning dynamics.

In fact, several proposals have been reported for performing bimodal cavity experiments [11, 12, 13, 14, 15, 16, 17]. In the proposal by Zubairy *et al* [13], for instance, a bimodal cavity is utilized to realize a quantum phase gate in which the two qubits are given by the cavity modes. Based on this gate, the authors suggested a scheme that enables one to implement Grover’s search algorithm. Another fruitful branch of the bimodal cavity applications represent proposals [14, 15, 16, 17], where the schemes for engineering of various entangled states between the atomic and/or photonic qubits have been reported. All these papers ignore, however, the effects of the ‘non-instantaneous’ detuning of the atom-cavity interaction from one cavity mode to the other, as well as the effective interaction among the cavity modes. Further investigation are therefore required to better understand how well these schemes may work in practise. Finally, we mention the papers [11, 12] where it has been proven that the coupling of both cavity modes to a common reservoir, as in line with $H_{coupled}$ (39), induces the tunneling of a field state from one cavity mode to another mode of the same cavity, and thus, opens a way to implement the environment assisted (short-distance) teleporting inside a bimodal cavity. We note that in order to follow the time evolution of such quantum systems embedded into a reservoir or under the external noise and to analyze different (entanglement or separability) measures, a ‘quantum simulator’ has been developed recently in our group [21] that can be utilized for such studies in the future.

Acknowledgments

We acknowledge the fruitful discussion with Thomas Radtke. This work was supported by the Deutsche Forschungsgemeinschaft (DFG).

References

- [1] Einstein A, Podolsky B and Rosen N 1935 *Phys. Rev.* **47** 777
- [2] Nielsen M A and Chuang I L 2000 *Quantum Computation and quantum Information* (Cambridge: Cambridge University Press)
- [3] Bennett C H and Wiesner S J 1992 *Phys. Rev. Lett.* **69** 2881
- [4] Ekert A K 1991 *Phys. Rev. Lett.* **67** 661
- [5] Grover L K 1997 *Phys. Rev. Lett.* **79** 325

- [6] Raimond J M, Brune M and Haroche S 2001 *Rev. Mod. Phys.* **73** 565
- [7] Kuhr S et al. 2007 *Appl. Phys. Lett.* **90** 164101
- [8] Rauschenbeutel A, Bertet P, Osnaghi S, Nogues G, Brune M, Raimond J M and Haroche S 2001 *Phys. Rev. A* **64** 050301
- [9] Haroche S and Raimond J M 2006 *Exploring the Quantum: Atoms, Cavities, and Photons* (Oxford: Oxford University Press)
- [10] Bosco de Magalhaes A R and Nemes M C 2004 *Phys. Rev. A* **70** 053825
- [11] Iara de Queirs P, Souza S, Cardoso W B and de Almeida N G 2007 *Phys. Rev. A* **76** 034101
- [12] Bosco de Magalhaes A R and Nemes M C 2005 *Phys. Lett. A* **339** 294
- [13] Zubairy M S, Kim M and Scully M O 2003 *Phys. Rev. A* **68** 033820
- [14] Biswas A and Agarwal G S 2004 *J. of Modern Optics* **51** 1627
- [15] Zou X and Mathis W 2005 *J. of Modern Optics* **52** 2001
- [16] Ikram M and Saif F 2002 *Phys. Rev. A* **66** 014304
- [17] Wildfeuer C and Schiller D H 2003 *Phys. Rev. A* **67** 053801
- [18] Jaynes E T and Cummings F W 1963 *Proc. IEEE* **51** 89
- [19] Puri R R 2001 *Mathematical Methods of Quantum Optics* (Berlin: Springer).
- [20] Maitre X, Hagley E, Nogues G, Wunderlich C, Goy P, Brune M, Raimond J M and Haroche S 1997 *Phys. Rev. Lett.* **79** 769
- [21] Radtke T and Fritzsche S, 2006 *Comput. Phys. Commun.* **175** 145; *ibid.* **176** 617